American Mineralogist, Volume 75, pages 687–693, 1990

Low temperature alteration of REE-rich chlorapatite from the Stillwater Complex, Montana

A. E. Boudreau
Department of Geology, Duke University, Durham, North Carolina 27706, U.S.A.
I. S. McCallum
Department of Geological Sciences, AJ-20, University of Washington, Seattle, Washington 98195, U.S.A.

Abstract

Chlorapatite is associated with coarse-grained olivine-rich rocks that host platinum-group element-bearing sulfide mineralization of the J-M Reef of the Stillwater Complex. The chlorapatite may contain in excess of 2 wt% of rare-earth elements (REE). The high-temperature magmatic-hydrothermal assemblage has undergone various degrees of serpentinization. A Cl-poor, very finely intergrown alteration assemblage occurs as pseudomorphs of, and along healed fractures in individual grains of primary chlorapatite. The alteration assemblage includes hydroxyapatite (which may contain up to 10% carbonate substituting for phosphorus), monazite, and undifferentiated silicates and oxides. The early stage of alteration is marked by the leaching of REE and their precipitation as monazite prior to extensive loss of Cl from the host chlorapatite. The progressive destruction of chlorapatite led to increased chlorinity and acidity of the solution at the reaction front, which, in turn, enhanced the dissolution of monazite. The textural and compositional features demonstrate that the replacement of chlorapatite by hydroxyapatite occurs through recrystallization, and they imply that chlorapatites are resistant to reequilibration of low temperature by diffusive processes. REE locally may be remobilized (on the grain-size scale) owing to the increase in solution acidity accompanying the destruction of chlorapatite.

Introduction

The halogen-bearing minerals associated with the major platinum-group element (PGE) deposit of the Stillwater Complex, the J-M Reef, are unusual in that they contain high Cl and REE concentrations (Boudreau et al., 1986; Boudreau and McCallum, 1989). Apatite with such high-Cl concentrations is rare in terrestrial igneous rocks in general and in layered igneous intrusions in particular (e.g., Nash, 1984; Boudreau et al., 1986). We report here textural and compositional observations regarding the alteration of primary chlorapatite during serpentinization.

Petrography

Apatite occurs as a minor phase throughout the Stillwater Complex and associated rocks (Boudreau and McCallum, 1989). Cl-rich apatite is characteristic of the lower third of the complex, above the Basal series. Within the platiniferous J-M Reef in olivine-bearing zone I (OBI) of the Banded series, chlorapatite is commonly present in coarse-grained to pegmatitic olivine-bearing rocks that also contain phlogopite. The chlorapatite grains range from several tens of micrometers to about 1 mm in size, and occur interstitial to cumulate and postcumulate silicates and chromite. The primary chlorapatite contains multiphase hydrous silicate inclusions (typically pargasite and phlogopite), which we interpreted to be the crystallization products of primary inclusions of hydrous silicate melt (Boudreau et al., 1986).

All the rocks have undergone variable degrees of zeolite-facies to lower greenschist-facies metamorphism, the most obvious result of which is the partial alteration of olivine to serpentine + magnetite ± calcite. The alteration is often mineral-specific, affecting olivine much more readily than either plagioclase or pyroxene. In the Ultramafic Series of the Stillwater Complex, Page (1976) identified lizardite and chrysotile (after olivine) and thompsonite or other zeolites (after plagioclase) as the most abundant alteration minerals. Temperatures for the alteration were estimated to be on the order of 100 °C, based on thermal estimates for similar assemblages found elsewhere. This temperature should be considered a minimum, as elsewhere in the Stillwater Complex (particularly proximal to dike intrusions) the alteration assemblage is characteristic of greenschist-facies metamorphism (e.g., McCallum et al., 1980).

Reaction of chlorapatite with low-temperature fluids resulted in the formation of a poorly crystallized and inclusion-filled hydroxyapatite, which occurs both as healed fractures a few tens of micrometers wide and as larger areas of partial to complete pseudomorphs after chlorapatite (Fig. 1). The microfractures, formed during tectonism and serpentinization, cross grain boundaries. A decrease in the chlorapatite component in the igneous apatite

0003–004X/90/0506–0687$02.00

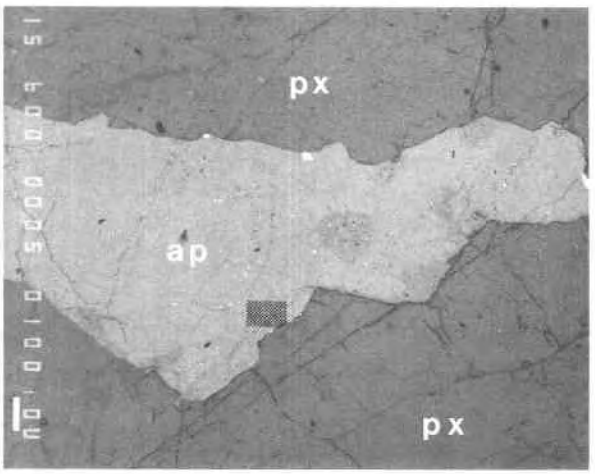

Fig. 1. Backscattered electron image of chlorapatite (ap), interstitial to orthopyroxene (px) in harzburgite from the J-M Reef, Minneapolis adit area. The slightly darker gray patches within the chlorapatite are regions of alteration. The bright spots that occur along the grain margins and as trails within the chlorapatite are mainly monazite and minor Fe-oxide. The shaded area shows the region of the X-ray maps of Fig. 3. Scale bar is 100 μm.

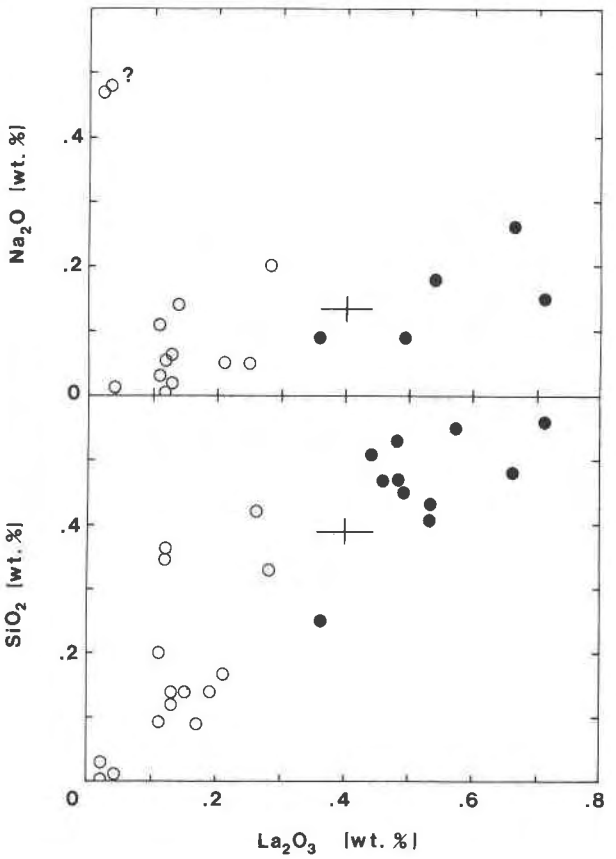

Fig. 2. Plot of SiO_2 and Na_2O against La_2O_3 (in wt%) in Cl-rich apatites from olivine-bearing zone I (OB I) of the Stillwater Complex. Closed circles are analyses of grain shown in Fig. 1; open circles are analyses of other samples. Error bars are typical 2σ counting-statistics errors. Note two anomalous high Na samples.

along the reaction front is evident from its higher birefringence relative to adjacent chlorapatite (Deer et al., 1966). A discolored-to-opaque appearance of both the microveins and the larger alteration patches results from numerous very fine inclusions of monazite, iron-oxide, and a variety of unidentified minerals associated with the replacement. The presence of inclusion "trails" of monazite further defines the healed fractures within the chlorapatite host. Except for the scale, the veining is similar in appearance to the low-Cl apatite veining in chlorapatite reported by Morton and Catanzaro (1964). The association of monazite with alteration suggests that the monazite is neither a primary igneous mineral nor an exsolution feature but instead formed as REE and Y were liberated from chlorapatite during alteration. In this regard, the monazite is similar to secondary monazite associated with secondary hexagonal apatite formed by the weathering of carbonatite, as reported by Lottermoser (1988).

Geochemistry

Methods

Electron microprobe analyses were carried out on a JEOL 733 automated four-spectrometer electron microprobe. Standard analysis conditions were 15-kv acceleration potential and counting times of 10–40 s. For compositional traverses, a 10-nA beam current and focused beam were used; for analysis of the more homogeneous areas, a 10-μm beam and 25-nA beam current were used. Standards include natural chlorapatite (RM-1, Morton and Catanzaro, 1964) and fluorapatite (Wilburforce) for Ca, P, and the halogens, and synthetic glasses and allanite (102522, #42; Frondel, 1964) for the REE. Data were corrected using a Tracor-Northern ZAF correction program. X-ray emission lines used for analysis and 3σ detection limits for the REE (wt%) are as follows: La $L\alpha_1$ (0.04), Ce $L\alpha_1$ (0.03), Pr $L\beta_1$ (0.08), Nd $L\alpha_1$ (0.04), Sm $L\alpha_1$ (0.06), Eu $L\beta_1$ (0.10), Gd $L\beta_2$ (0.25), Dy $L\alpha_1$ (0.06), Er $L\alpha_1$ (0.05), Yb $L\alpha_1$ (0.06). The maximum overlap on Eu, Dy, Er, and Yb lines is $\leq$10% (Roeder, 1985); in addition, the overlapping lines are from the heavy REE, whose low concentrations make the possible error for these elements less than the expected error of analysis.

Results

An electron-microprobe analysis of the unaltered part of the grain shown in Figure 1 is presented in Table 1. The host chlorapatite contains >2.0 wt% total REE. Positive correlations between the REE and SiO_2 concentrations (and somewhat poorer correlations between the REE and Na_2O) in primary chlorapatites from OB I (Fig. 2)

TABLE 1. Microprobe analysis of REE-rich chlorapatite of Figure 1

	wt%	ions per 26 (O, Cl, F, OH)	
SiO_2	0.56	0.098	
Al_2O_3	nd	—	
FeO	0.08	0.012	
MgO	nd	—	
MnO	0.03	0.004	
CaO	50.81	9.556	$\Sigma(P + Si) = 6.042$
SrO	nd	—	
Na_2O	0.15	0.050	$\Sigma(REE + Y + A^{2+}) = 9.828$
P_2O_5	40.00	5.944	
F	0.60	0.334	$\Sigma(F + Cl) = 2.080$
Cl	5.87	1.746	
H_2O^*	0.00	—	$\Sigma(REE + Y) = 0.204$
La_2O_3	0.71	0.046	
Ce_2O_3	1.28	0.082	$\Sigma(Si + Na) = 0.148$
Pr_2O_3	0.19	0.012	
Nd_2O_3	0.59	0.038	
Sm_2O_3	0.09	0.006	
Eu_2O_3	nd	—	
Gd_2O_3	nd	—	
Dy_2O_3	0.10	0.006	
Er_2O_3	nd	—	
Yb_2O_3	nd	—	
Y_2O_3	0.17	0.016	
Total	101.23		
O ≡ F, Cl	1.58		
Total	99.66		

Note: Abbreviation: nd = not detected.

* OH and H_2O calculated on the basis of Cl + F + OH = 2.0 in anion site.

TABLE 2. Microprobe analysis of apatite that replaces chlorapatite, grain of Figure 1

	1.*		2.	
	wt%	ions per 26 anions	wt%	ions per 26 anions
SiO_2	0.25	0.042	0.12	0.020
FeO	0.20	0.028	0.52	0.072
MgO	0.11	0.028	0.00	0.000
CaO	54.50	9.994	55.16	9.896
P_2O_5	38.74	5.614	37.54	5.322
F	0.16	0.086	0.47	0.248
Cl	4.03	1.168	2.23	0.632
CO_2**	1.45	0.338	2.90	0.662
H_2O†	0.94	1.074	1.59	1.778
La_2O_3	0.16	0.010	0.05	0.004
Total	100.43		100.69	
O ≡ F, Cl	0.98		0.70	
Total	99.45		99.99	
Σ(P + C + Si)		5.996		6.004
C/(P + C + Si)		0.056		0.110
Σ(Cl + F + OH − C)		1.992		1.998

* Apatite analysis at reaction front with host chlorapatite.

** CO_2 calculated on the basis of (P + Si + C) = 2 per 26 anions.

† H_2O calculated on the basis of anion site difference and on the assumption that carbonate substitutes as $(CO_3 \cdot OH)^{3-}$; e.g., (OH + Cl + F) = (2 + C) per 26 anions. For both H_2O and CO_2, the estimates are improved by iterative calculation; i.e., H_2O and CO_2 estimates are used in new formula calculations of ion site requirements.

agree with previous studies (e.g., Ito, 1968; Roeder et al., 1987; Rønsbo, 1989) which suggest that the coupled substitutions $Ca^{2+} + P^{5+} = REE + Si^{4+}$ and $2Ca^{2+} = Na^+ + REE^{3+}$ are the principal mechanisms by which the REE substitute in the apatite structure. Furthermore, these exchanges appear to be independent of the halogen species filling the anion site, as trends similar to those of Figure 2 for REE substitution in fluorapatites have been reported by Rønsbo (1989).

Details of Cl and Ce distribution in areas in which the chlorapatite has undergone alteration are shown in the X-ray maps in Figure 3. Monazite inclusions most commonly occur in linear trains and in patches, around which the host chlorapatite is depleted in REE. These same regions are also poor in Cl locally, but not everywhere. Many of the Cl-poor regions contain little monazite. A compositional traverse across a microvein (Fig. 4) shows that Cl and La decrease abruptly, whereas Si, Fe, and Mg increase, toward the center of the vein. An apparent maximum in La concentration occurs on both sides of the microvein. These observations lead to the conclusion that monazite formed prior to extensive loss of Cl from the chlorapatite, i.e., REE concentrations in the infiltrating fluid are highest early in the alteration process.

Microprobe analysis of the alteration assemblage shows the chlorapatite to be replaced largely by fine-grained apatite (Table 2) in which the decrease of Cl and increase in OH becomes more pronounced away from the reaction front. Accurate analysis of the replacement material is difficult owing to the possible substitution of both CO_2 and H_2O in the apatite structure. The substitution of carbonate $(CO_3)^{2-}$ for the $(PO_4)^{3-}$ group is likely to be complex because of the need for charge-balance requirements that may involve excess OH^- (Nathan, 1984; LeGeros and LeGeros, 1984). The calculated CO_2 and H_2O in Table 2 are based on the assumption that the carbonate substitution is $(CO_3 \cdot OH)^{3-} = (PO_4)^{3-}$ and that F + Cl + OH = 1 in the anion site, although some monovalent cations substituting for Ca may also accompany the substitution of $(CO_3)^{2-}$ for $(PO_4)^{3-}$. The estimated CO_2 contents listed in Table 2 are similar to those reported in carbonate fluorapatites in sedimentary phosphorites (e.g., Nathan, 1984) but are slightly low for the range reported by Nriagu (1984) for carbonate apatites in general. It is thus reasonable that the replacement apatite may contain up to 10 mol% of the carbonate-hydroxyapatite endmember (dahllite). Typically, however, the alteration material is too finely intergrown to allow microprobe analysis of individual replacement apatite grains.

The monazite grains contain little other than P, REE, Th, and Y (Table 3). Chondrite-normalized REE concentration patterns of the unaltered chlorapatite and the secondary monazite both show light REE (LREE) enrichment, a feature typical of monazite in general (Nash, 1984) (Fig. 5). The monazite has an apparent negative Eu anomaly of uncertain magnitude (Eu below detection limits), which might have been inherited from the chlorapatite from which it formed. Also, relative to the distribution in chlorapatite, monazite apparently takes up the light REE in preference to the heavy REE. No specifically HREE-rich

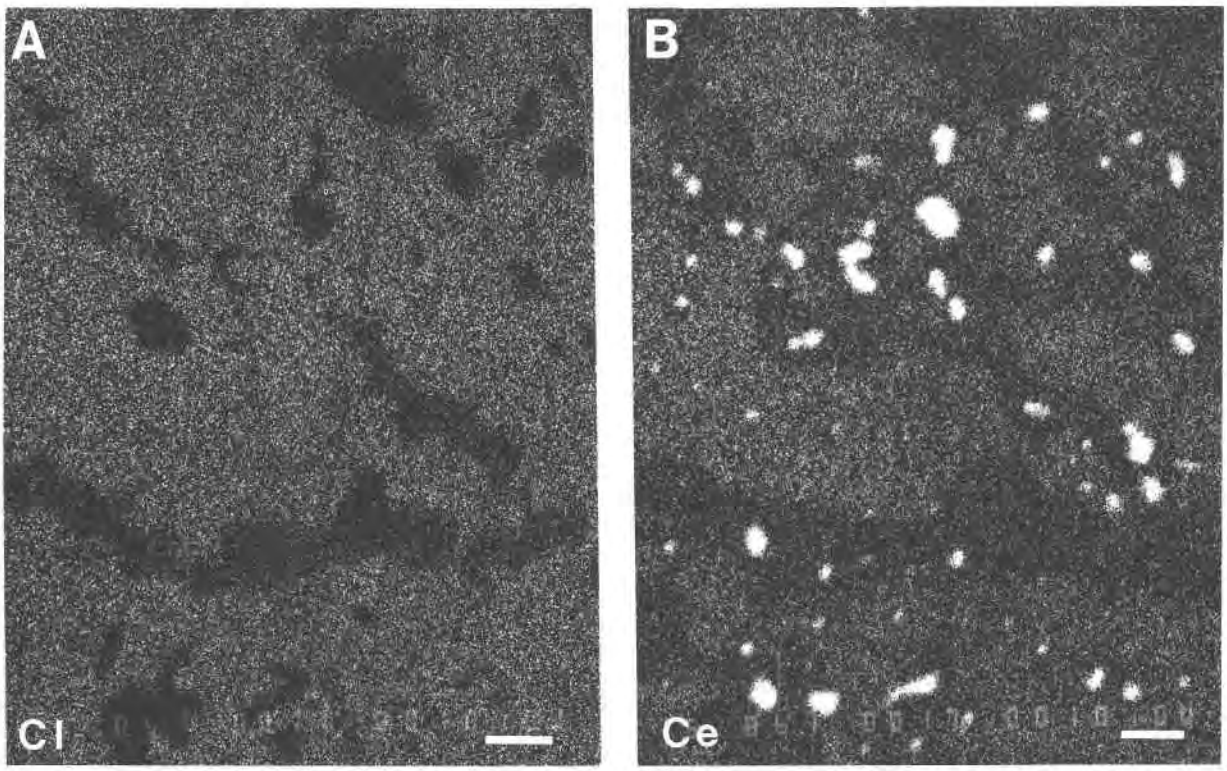

Fig. 3. X-ray maps of chlorapatite shown in shaded region of Fig. 1. (**A**) Cl distribution. (**B**) Ce distribution. Scale bar is 10 μm. Note uniform composition of chlorapatite in unaltered areas. See text for further discussion.

minerals (e.g., xenotime; Nash, 1984) were observed by energy-dispersive X-ray spectrometry, which might complement the LREE-rich monazite.

To summarize, alteration of primary chlorapatite resulted in the formation of monazite by leaching of the REE from the host chlorapatite prior to significant loss of Cl. As reaction progressed, chlorapatite was replaced by a poorly crystallized, Cl-poor alteration assemblage consisting of hydroxyapatite with up to 10 mol% dahllite component, monazite and silicate-oxide phases. The exchange of Cl for OH during the recrystallization appears to have increased the chlorinity of the infiltrating fluid such that REE solubility was locally enhanced. This resulted in the late redissolution of monazite and loss of REE. The presence of relatively large monazite grains at the margins of the original chlorapatite grain suggests that the mobility of the REE was limited and did not occur beyond the scale of the individual grain undergoing alteration.

Discussion

The above textural and compositional features are consistent with the interpretation that alteration of primary chlorapatite by an aqueous fluid results in a Cl-poor alteration assemblage. Estimates of changing HCl concentrations and solution acidity of the low-temperature fluid as it reacts with the chlorapatite can be calculated through exchange equilibria between apatite and infiltrating aqueous fluid:

$$\underset{\text{apatite}}{Ca_5(PO_4)_3OH} + \underset{\text{fluid}}{HCl} = \underset{\text{apatite}}{Ca_5(PO_4)_3Cl} + \underset{\text{fluid}}{H_2O}. \quad (1)$$

The equilibrium constant for Reaction 1 is given by

$$\log K_1 = \frac{a(Ca_5(PO_4)_3Cl)\cdot f(H_2O)}{a(Ca_5(PO_4)_3OH)\cdot f(HCl)}, \quad (2)$$

where a is the activity. Values for Equation 2 are given by the following expression (kindly supplied by R. C. Tacker and valid for temperatures from 25 to 400 °C):

$$\log K_1 = 7.972 - 0.009T(°C) + 9.522 \times 10^{-6}T^2 + (P - 1)(5.802 \times 10^{-4}). \quad (3)$$

If one assumes ideal behavior in the fluid solution and apatite solid solution, Equation 2 reduces to

$$\log K_1 = \frac{X(Ca_5(PO_4)_3Cl)\cdot X(H_2O)}{X(Ca_5(PO_4)_3OH)\cdot X(HCl)},$$

or,

$$\log X(HCl) = \log \frac{X(Ca_5(PO_4)_3Cl)}{X(Ca_5(PO_4)_3OH)} + \log X(H_2O) - \log K_1,$$

TABLE 3. Microprobe analysis of monazite after chlorapatite, from grain in Figure 1

	wt%	ions per 4 anions
SiO_2	0.21	0.008
Al_2O_3	nd	
FeO	0.15	0.005
MgO	nd	
MnO	nd	
CaO	0.25	0.010
SrO	nd	
Na_2O	nd	
P_2O_5	30.14	0.995
F	na	
Cl	nd	
La_2O_3	23.75	0.342
Ce_2O_3	31.28	0.446
Pr_2O_3	2.37	0.034
Nd_2O_3	8.43	0.117
Sm_2O_3	1.24	0.017
Eu_2O_3	nd	
Gd_2O_3	0.90	0.012
Dy_2O_3	0.25	0.003
Er_2O_3	nd	
Yb_2O_3	nd	
ThO_2	1.09	0.010
Y_2O_3	0.23*	0.005
Total	100.29	

Note: Σ(REE + Y + Th) = 0.986. Abbreviations: nd = not detected; na = not analyzed.
* Other monazite analyses contain as much as 2.88 wt% Y_2O_3.

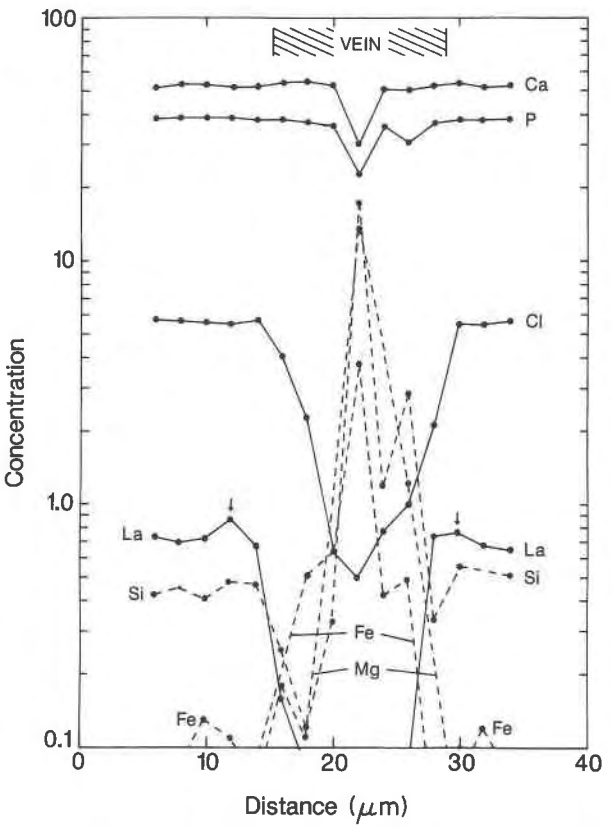

Fig. 4. Microprobe traverse across microvein in chlorapatite. Note logarithmic concentration scale. Solid lines are for elements depleted from both the chlorapatite and vein; dashed lines are for elements enriched in the vein. La concentrations tend to be highest immediately adjacent to vein (arrows), whereas Fe, Mg, and Si are concentrated in inclusions along the central axis of the vein.

where X is the mole fraction. Assuming dilute solutions (i.e., $X(H_2O) \cong 1$), then

$$\log X(\mathrm{HCl}) = \log \frac{X(\mathrm{Ca_5(PO_4)_3Cl})}{X(\mathrm{Ca_5(PO_4)_3OH})} - \log K_1. \quad (4)$$

In addition, the HCl will undergo dissociation via the reaction

$$\mathrm{HCl} = \mathrm{H^+} + \mathrm{Cl^-},$$

for which the dissociation constant is given by

$$\log K_{\mathrm{HCl}} = \log \frac{a(\mathrm{H^+})\cdot a(\mathrm{Cl^-})}{a(\mathrm{HCl})}. \quad (5)$$

In Equation 5, activity is typically expressed as a function of molality, e.g.,

$$a(\mathrm{HCl}) = \gamma(\mathrm{HCl})\cdot m(\mathrm{HCl}).$$

Again, assuming ideal, dilute solutions, then

$$a(\mathrm{HCl}) = m(\mathrm{HCl}) \approx X(\mathrm{HCl})\cdot 55.5,$$

or,

$$\log a(\mathrm{HCl}) \approx \log X(\mathrm{HCl}) + 1.74. \quad (6)$$

Substitution of Equations 4 and 6 into Equation 5 and solving for $a(H^+)$, one arrives at

$$\log a(\mathrm{H^+}) = \log K_{\mathrm{HCl}} - \log a(\mathrm{Cl^-}) + 1.74 + \log \frac{X(\mathrm{Ca_5(PO_4)_3Cl})}{X(\mathrm{Ca_5(PO_4)_3OH})} - \log K_1. \quad (7)$$

One can thus calculate solution acidity, provided an independent estimate of $a(Cl^-)$ is known. Equation 7 has been solved using Equation 3 for $\log K_1$, $a(Cl^-) = 1.0$, and for mole fractions of chlorapatite = 0.9, 0.5, and 0.1, respectively (Fig. 6). In addition, the values of Henley (1984) were used for the dissociation constant for HCl in the temperature interval 50 to 300 °C at vapor-saturated pressures (1 to 86 bars). The dissociation constants for HCl over this temperature interval range from −0.03 at 100 °C and 1 bar pressure to −1.37 at 300 °C, 86 bars pressure; i.e., HCl becomes less dissociated with increasing temperatures. Also plotted in Figure 6 is the neutral pH of pure water as a function of temperature.

The lack of extensive alteration in the primary silicates other than olivine suggests that the infiltrating solutions were not particularly acid initially. However, the reaction of chlorapatite with an otherwise neutral pH aqueous fluid would force reaction 1 to the left and lead to increased HCl concentrations in the fluid. This increase in solution acidity and chlorinity would favor the transport of REE, thus explaining the lack of monazite in regions of exten-

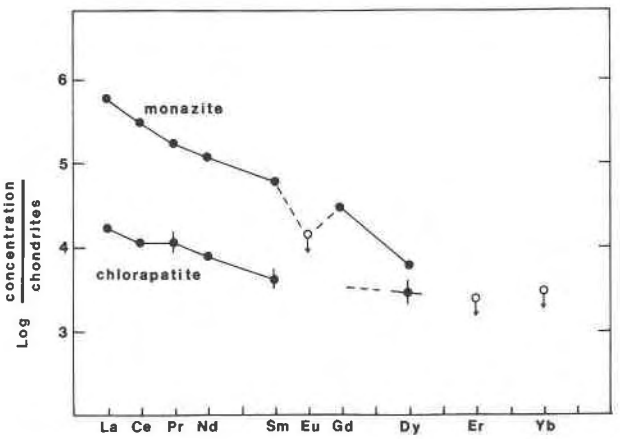

Fig. 5. Chondrite-normalized plot of REE abundances in monazite and host chlorapatite. Open circles with arrows are microprobe detection limits for those elements in monazite whose abundances are below detection limits. Error bars are shown for those concentrations for which the error is larger than the symbol size.

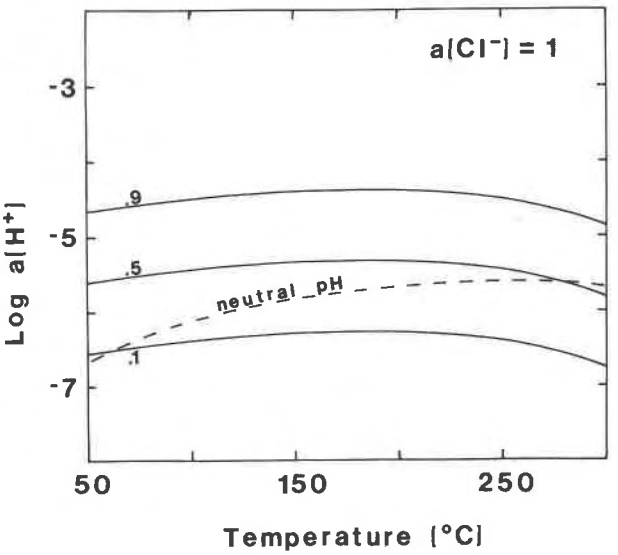

Fig. 6. Calculated log $a(H^+)$ as a function of temperature at vapor-saturated pressures for the value of $a(Cl^-) = 1.0$ for a fluid in equilibrium with chlorapatite-hydroxyapatite solid solution. Solid lines are plots of hydrogen activity as a function of temperature for values of the mole fraction of chlorapatite in the chlorapatite-hydroxyapatite solid solution as shown. Dashed line is the neutral pH for pure water as a function of temperature. See text for other assumptions used in calculation.

sive Cl loss. It is concluded that the high HCl concentrations are a localized phenomenon accompanying the low-temperature replacement reaction, similar to the Cl enrichment that occurs at reaction fronts associated with the serpentinization of olivine (e.g., Rucklidge and Patterson, 1977). In addition, the convergence at low temperature of the neutral pH line with a solution in equilibrium with apatite having low Cl content is consistent with a low temperature (~100 °C) of formation for the hydroxyapatite from neutral meteoric water. Although this convergence is fortuitous, in part, owing to the arbitrary value selected for chloride activity, an initially low acidity in the infiltrating fluid is consistent with the apparent limited mobility of the REE noted earlier.

Although the above conclusions are in agreement with textural and compositional observations, the calculations used to derive Figure 6 must include the following caveats. Apatite Cl-OH solid solution is likely to become nonideal at temperatures below approximately 400 °C, and both chlorapatite and hydroxyapatite exhibit a transition from monoclinic to hexagonal forms at temperatures around 200 °C (Tacker and Stormer, 1989; Hughes et al., 1989). However, the degree of nonideality in the apatite Cl-OH solid solution is less than 5 kcal/mol at 25 °C (Duff, 1972). Also, the possibility of exchange reactions involving HF were ignored owing to the low F concentrations in both the primary and secondary apatite, although the low F content of both the high- and low-temperature apatites suggests that HF was not significant relative to HCl or H_2O in either environment. Finally, the possibility of substantial $(CO_3)^{2-}$ substitution into the hydroxyapatite implies some CO_2 component in the infiltrating fluid. Regardless of the uncertainty in the absolute value of the pH presented in Figure 5, the conclusion that the alteration of chlorapatite must entail a decrease in solution pH at the reaction front should remain generally valid.

Conclusions

Part of the aim of this study was to differentiate those features indicative of a high-temperature magmatic-hydrothermal event from the low-temperature serpentinization that has affected almost all olivine-bearing rocks of the Stillwater Complex to some degree. All available evidence indicates that Stillwater chlorapatite is a product of high-temperature magmatic-hydrothermal activity (e.g., Boudreau and McCallum, 1989) and is not a consequence of low-temperature serpentinization. The introduction of low-temperature fluids into the Stillwater Complex during post-crystallization tectonic-metamorphic events resulted in the replacement of chlorapatite by a Cl-poor assemblage consisting of monazite and a fine-grained, intimate mixture of hydroxyapatite and unidentified silicates-oxides. The replacement hydroxyapatite may contain up to 10 mol% of the carbonate apatite end-member (dahllite) and only minor REE. The sharp change in the compositional profile across the reaction front, as well as the poorly crystallized nature of the alteration assemblage, supports the conclusions of other studies (e.g., Tacker and Stormer, 1989, and summaries of earlier studies therein) that the halogens in apatite reequilibrate by recrystallization and not by diffusive exchange.

The destruction of chlorapatite by an infiltrating, neutral aqueous fluid resulted in the local generation of high

chloride and acid solutions that enhanced the leaching of the REE. The presence of relatively large monazite grains along the margins of the altered chlorapatite suggests, however, that REE remobilization is limited to the chlorapatite grain itself, as any low pH fluid produced by the alteration of chlorapatite would presumably be neutralized by reaction with surrounding silicates. Hence, it does not appear that any significant amounts of REE are lost from REE-rich, chlorapatite-bearing rocks undergoing partial alteration.

Acknowledgments

This work was supported by Grant EAR 8803340 from the National Science Foundation. Careful reviews and suggested additional references by C. Tacker (who supplied the expression used in Equation 3), P. Roeder, and P. Candela are gratefully acknowledged.

References cited

Boudreau, A.E., Mathez, E.A., and McCallum, I.S. (1986) Halogen geochemistry of the Stillwater and Bushveld Complexes: Evidence for transport of the platinum-group elements by Cl-rich fluids. Journal of Petrology, 27, 967–986.

Boudreau, A.E., and McCallum, I.S. (1989) Investigations of the Stillwater Complex, part V: Apatites as indicators of evolving fluid composition. Contributions to Mineralogy and Petrology, 102, 138–153.

Deer, W.A., Howie, R.A., and Zussman, J. (1966) An introduction to the rock-forming minerals, 528 p. Wiley, New York.

Duff, E.J. (1972) Orthophosphates IX: Chlorapatite: Phase relationships under aqueous conditions along the $Ca_5F(PO_4)$-$Ca_5Cl(PO_4)_3$ and $Ca_5OH(PO_4)$-$Ca_5Cl(PO_4)_3$ joins the system CaO-$CaCl_2$-CaF_2-P_2O_5-H_2O. Journal of Inorganic and Nuclear Chemistry, 34, 859–871.

Frondel, J.W. (1964) Variations of some rare earths in allanite. American Mineralogist, 49, 1159–1177.

Henley, R.W. (1984) pH calculations for hydrothermal fluids. In R.W. Henley, A.H. Truesdell, and P.B. Barton, Eds. Reviews in Economic Geology, v1: Fluid-mineral equilibria in hydrothermal systems, p. 83–98. Society of Economic Geology, El Paso, Texas.

Hughes, J.M., Cameron, M., and Crowley, K.D. (1989) Structural variations in natural F, OH, and Cl apatites. American Mineralogist, 74, 870–876.

Ito, J. (1968) Silicate apatites and oxyapatites. American Mineralogist, 53, 890–907.

LeGeros, R.Z., and LeGeros, J.P. (1984) Phosphate minerals in human tissues. In J.O. Nriagu and P.B. Moore, Eds., Phosphate minerals, p. 351–385. Springer-Verlag, New York.

Lottermoser, B.G. (1988) Supergene, secondary monazite from the Mt Weld carbonatite laterite, Western Australia. Neues Jahrbuch für Mineralogie Monatshefte, 2, 67–70.

McCallum, I.S., Raedeke, L.D., and Mathez, E.A. (1980) Investigations of the Stillwater Complex, part I: Stratigraphy and structure of the Banded zone. American Journal of Science, 280A, 59–87.

Morton, R.D., and Catanzaro, E.J. (1964) Stable chlorine isotope abundances in apatites from Odegårdens Verk, Norway. Norsk Geologisk Tidsskrift, 44, 307–313.

Nash, W.P. (1984) Phosphate minerals in terrestrial igneous and metamorphic rocks. In J.O. Nriagu and P.B. Moore, Eds., Phosphate minerals, p. 215–241. Springer-Verlag, New York.

Nathan, Y. (1984) The mineralogy and geochemistry of phosphorites. In J.O. Nriagu and P.B. Moore, Eds., Phosphate minerals, p. 275–291. Springer-Verlag, New York.

Nriagu, J.O. (1984) Phosphate minerals: Their properties and general modes of occurrence. In J.O. Nriagu and P.B. Moore, Eds., Phosphate minerals, p. 1–136. Springer-Verlag, New York.

Page, N.J. (1976) Serpentinization and alteration in an olivine cumulate from the Stillwater Complex, southwestern Montana. Contributions to Mineralogy and Petrology, 54, 127–137.

Roeder, P.L (1985) Electron-microprobe analysis of minerals for rare-earth elements: Use of calculated peak-overlap corrections. Canadian Mineralogist, 23, 263–271.

Roeder, P.L., MacArthur, D., Ma, X.-P., Palmer, G.R., and Mariano, A.N. (1987) Cathodoluminescence and microprobe study of rare-earth elements in apatite. American Mineralogist, 72, 801–811.

Rønsbo, J.G. (1989) Coupled substitutions involving REEs and Na and Si in apatites in alkaline rocks from the Ilímaussaq intrusion, South Greenland, and petrological implications. American Mineralogist, 74, 896–901.

Rucklidge, J.C., and Patterson, G.C. (1977) The role of chlorine in serpentinization. Contributions to Mineralogy and Petrology, 65, 39–44.

Tacker, R.C., and Stormer, J.C. (1989) A thermodynamic model for apatite solid solutions, applicable to high-temperature geologic problems. American Mineralogist, 74, 877–888.

Manuscript received July 1, 1989
Manuscript accepted February 9, 1990